——Supporting Information——

Ionic transport in potential coating materials for Mg batteries

Tina Chen,[1,2] Gopalakrishnan Sai Gautam,[3#] and Pieremanuele Canepa[4*]

[1]Department of Materials Science and Engineering, University of California, Berkeley, Berkeley, CA, United States

[2]Materials Science Division, Lawrence Berkeley National Laboratory, Berkeley, CA, United States

[3]Department of Mechanical and Aerospace Engineering, Princeton University, Princeton, NJ, United States

[4]Department of Materials Science and Engineering, National University of Singapore, 9 Engineering Drive 1, Singapore

Corresponding authors: [#]gautam91@princeton.edu and *pcanepa@nus.edu.sg

S1 Mg^{2+} Migration Energy Paths

The following figures report the Mg^{2+} migration energies along the migration paths computed in all the coating materials considered in this investigation (summarized in Table 3 and Figure 3 of the main text). The zero of the migration energy in all plots is referenced to the lowest energy end-member structure. The migration barrier in all cases is taken as the difference between the lowest and highest energy states. Note that β-$MgSiN_2$, $Ia\bar{3}$-Mg_3P_2, and $Fm\bar{3}m$-Mg_2Si correspond to structures with Materials Project IDs of mp-3677, mp-2514, and mp-1367, respectively.

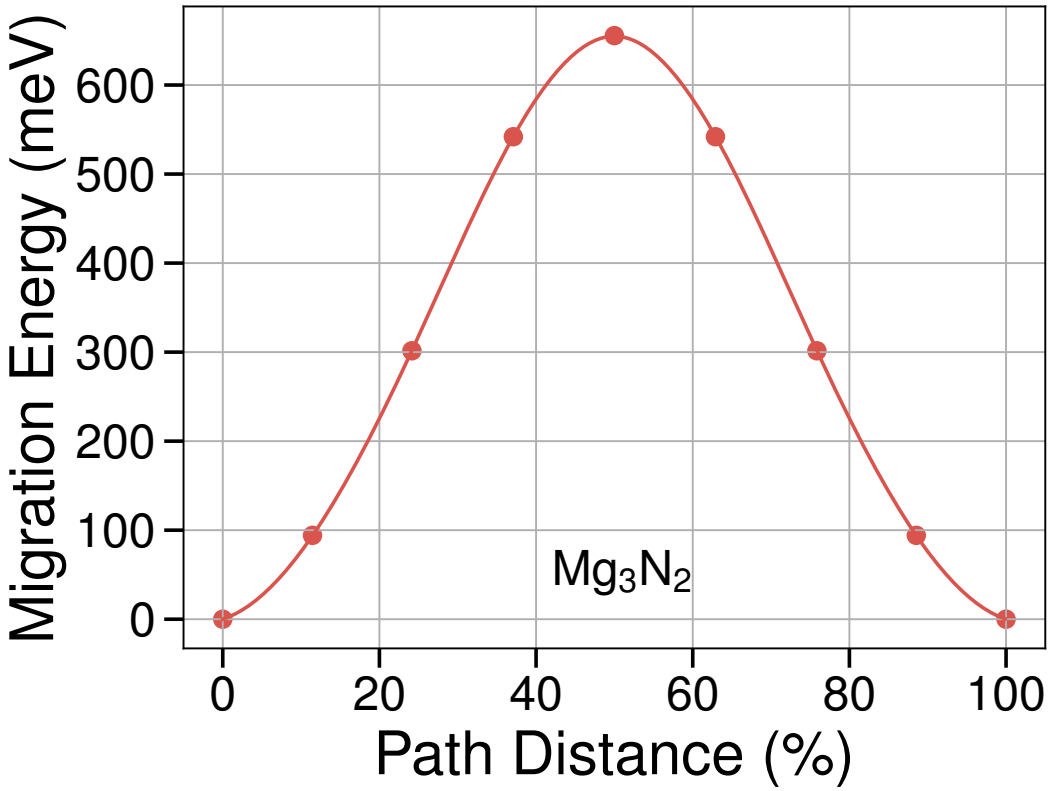

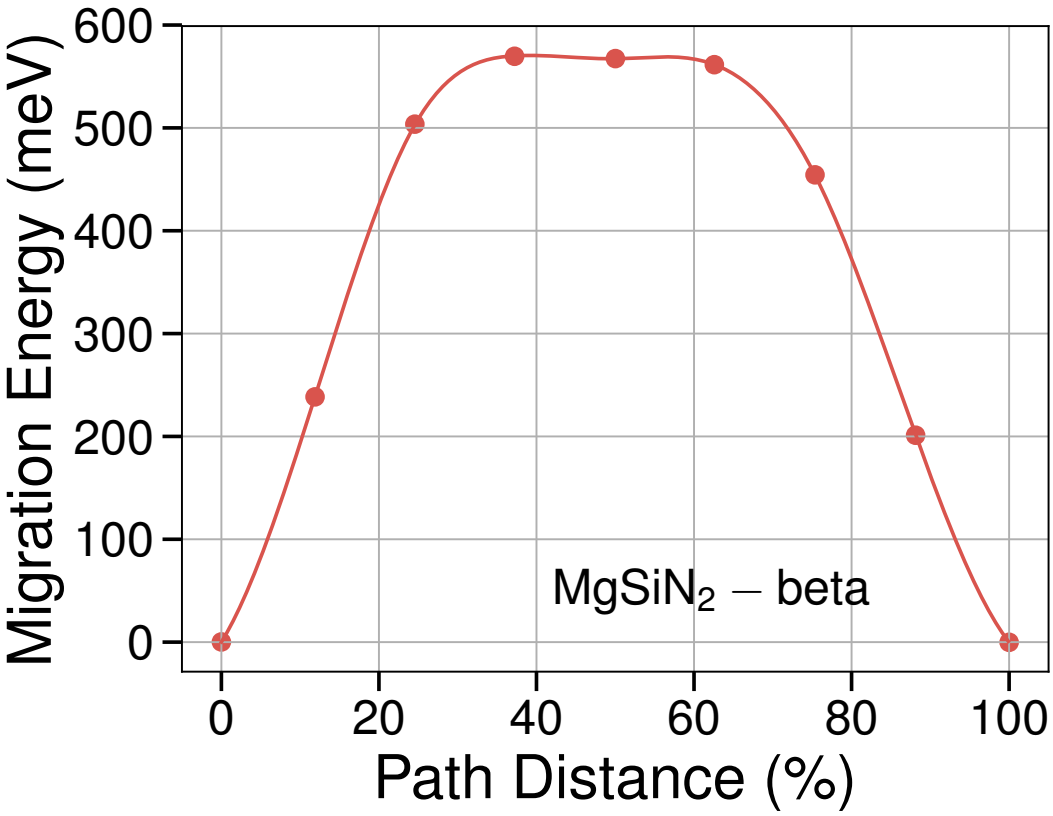
Migration Energy (meV)
600
500
400
300
200
100
0
0
20
40
60
80
100
Path Distance (%)
MgSiN2 – beta

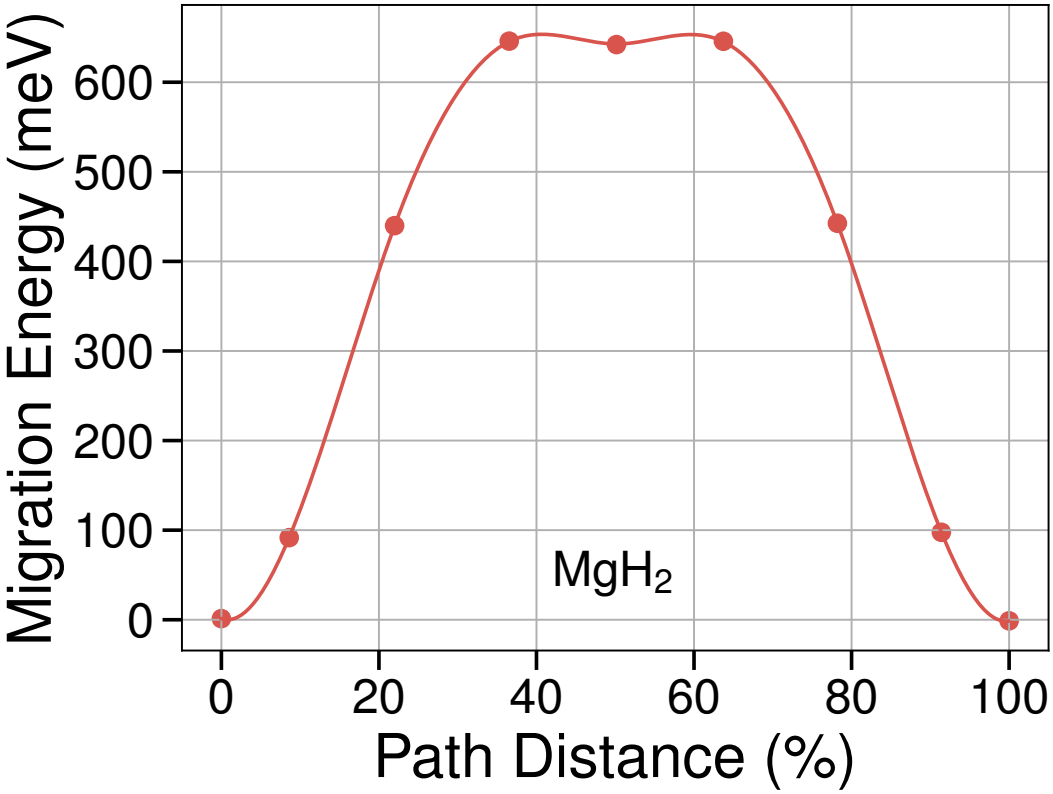
Migration Energy (meV)
600
500
400
300
200
100
0
0
20
40
60
80
100
Path Distance (%)
MgH2

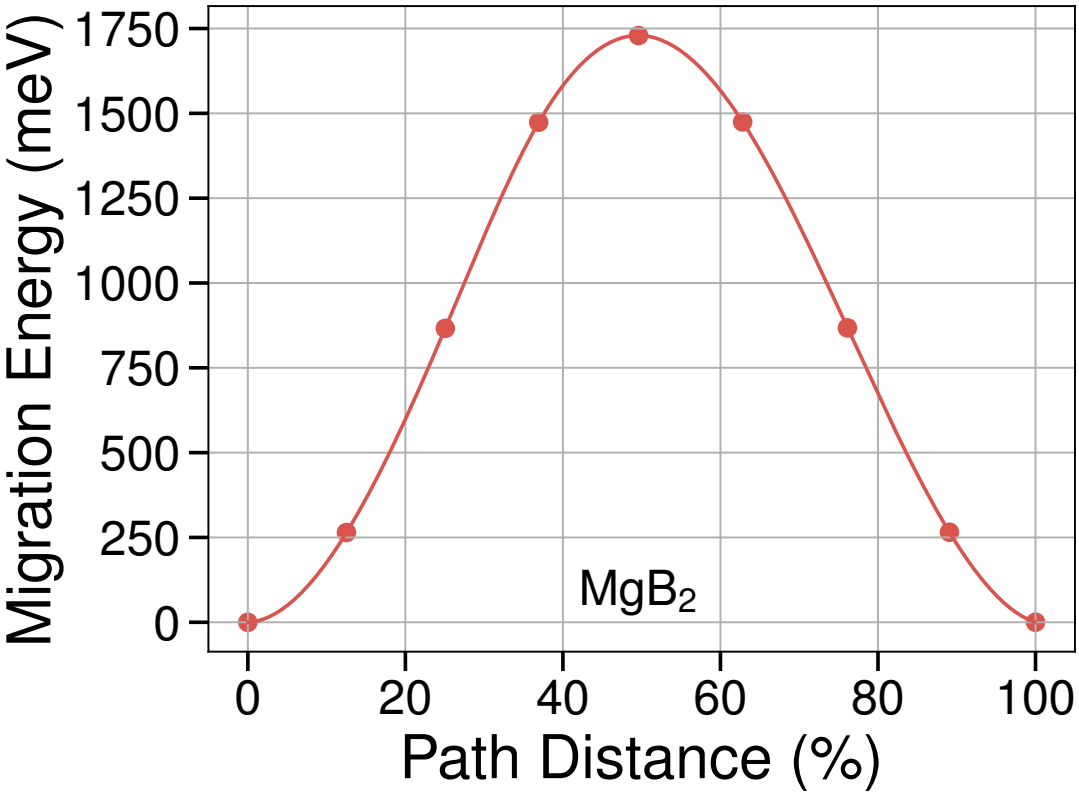
Migration Energy (meV)
1750
1500
1250
1000
750
500
250
0
MgB2
0
20
40
60
80
100
Path Distance (%)

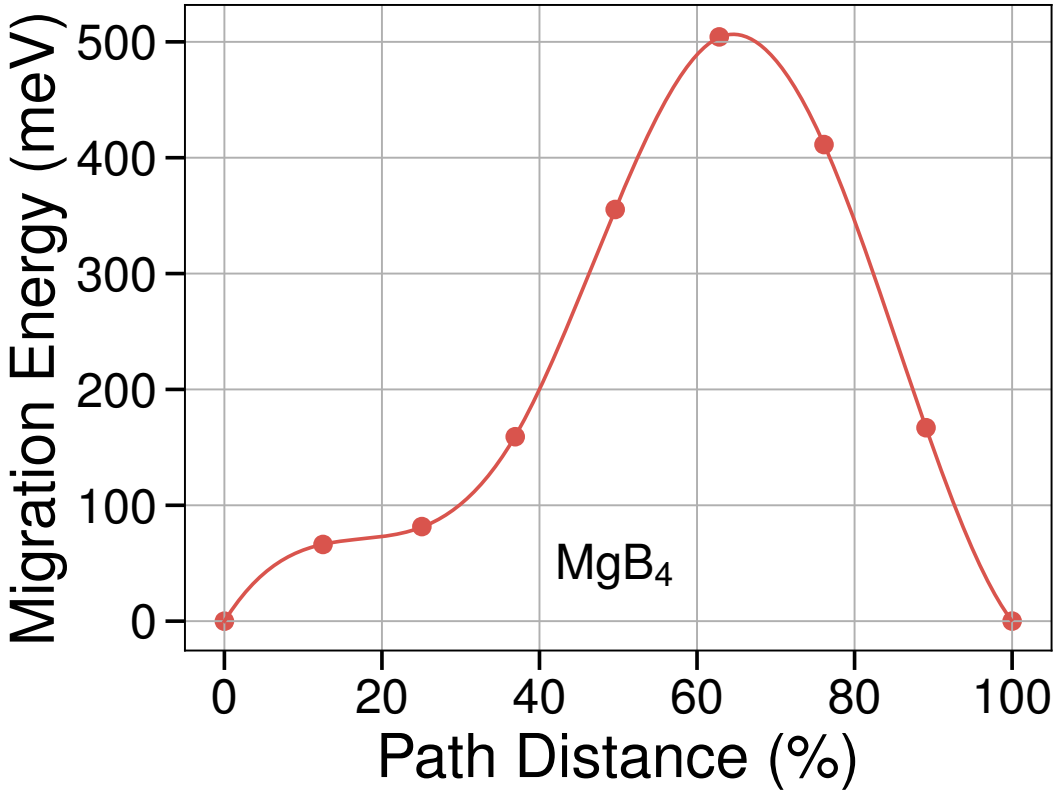
Migration Energy (meV)
500
400
300
200
100
0
MgB4
0
20
40
60
80
100
Path Distance (%)

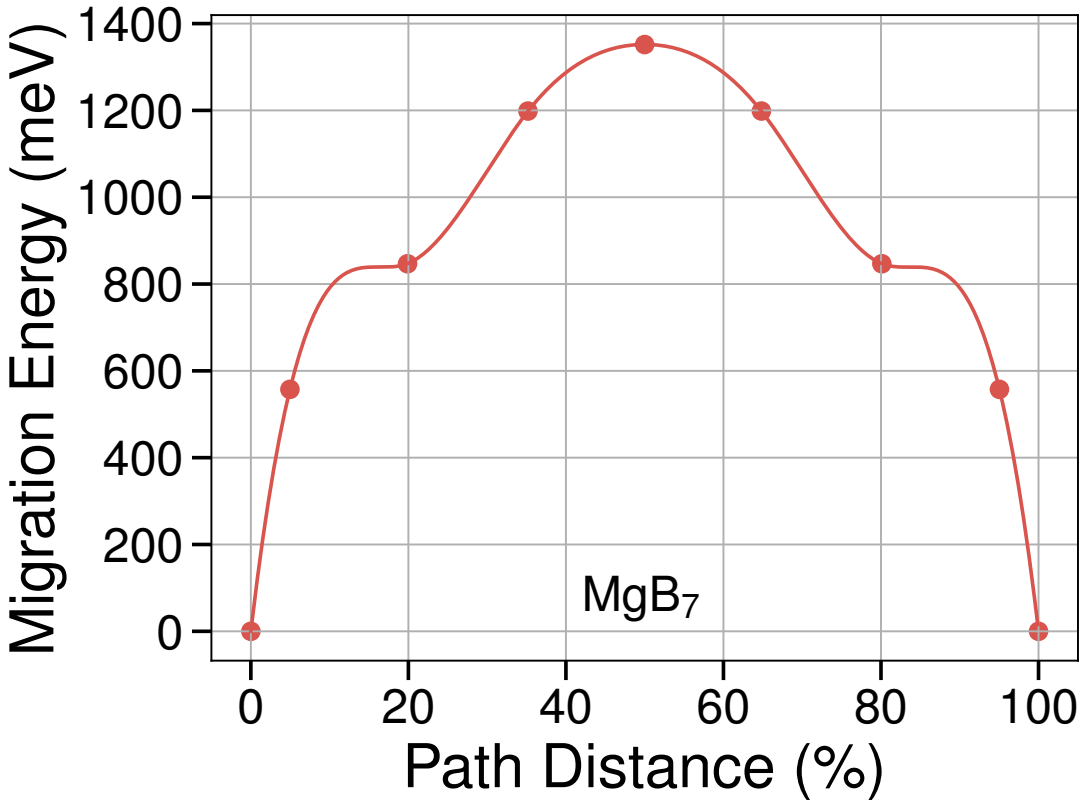
Migration Energy (meV)
1400
1200
1000
800
600
400
200
0
MgB7
0
20
40
60
80
100
Path Distance (%)

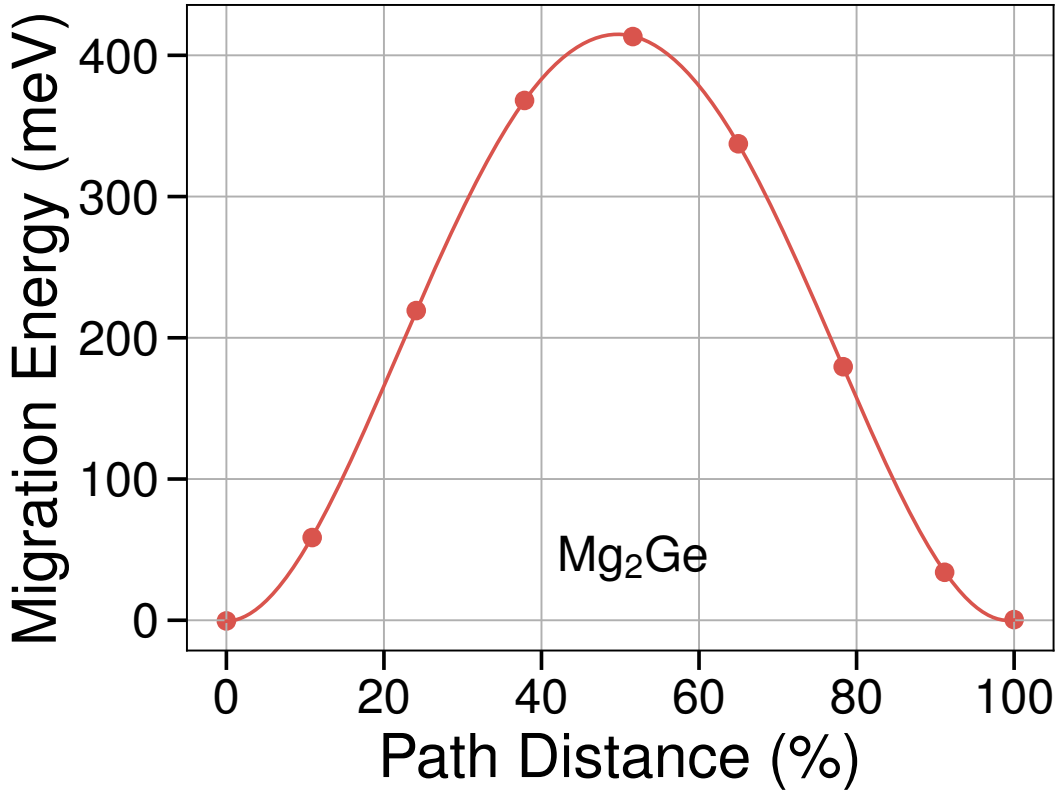
Migration Energy (meV)
400
300
200
100
0
Mg2Ge
0
20
40
60
80
100
Path Distance (%)

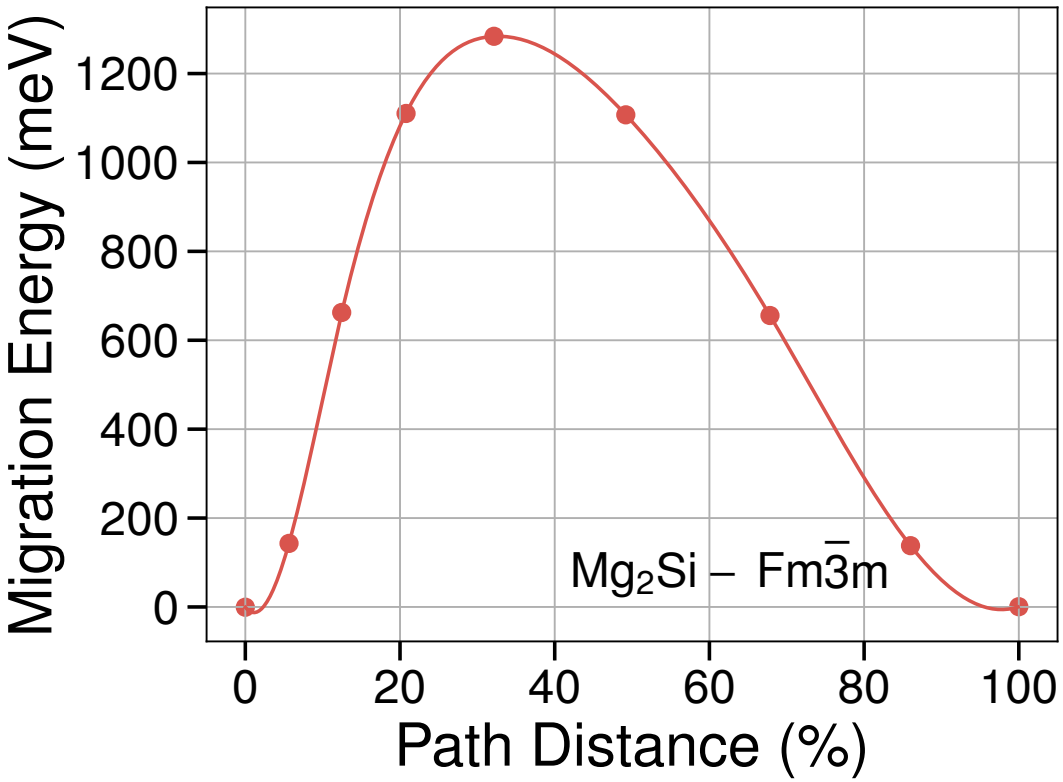
Migration Energy (meV)
1200
1000
800
600
400
200
0
0
20
40
60
80
100
Path Distance (%)
Mg2Si – Fm3̄m

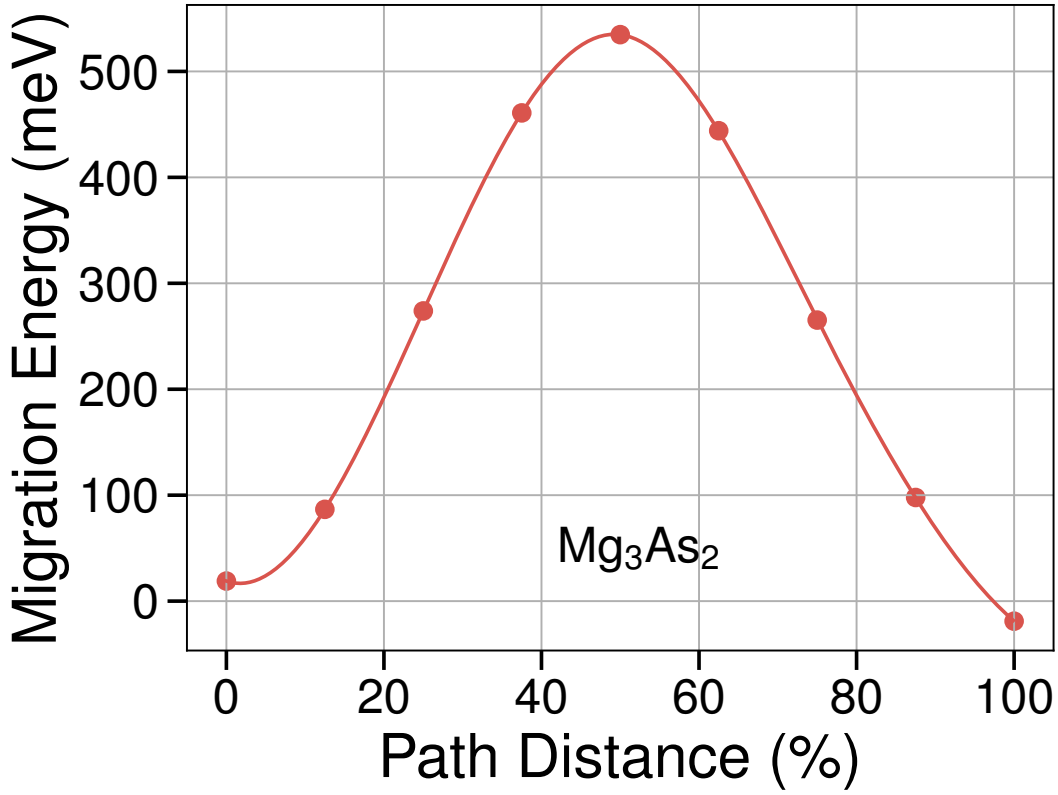
Migration Energy (meV)
500
400
300
200
100
0
0
20
40
60
80
100
Path Distance (%)
Mg3As2

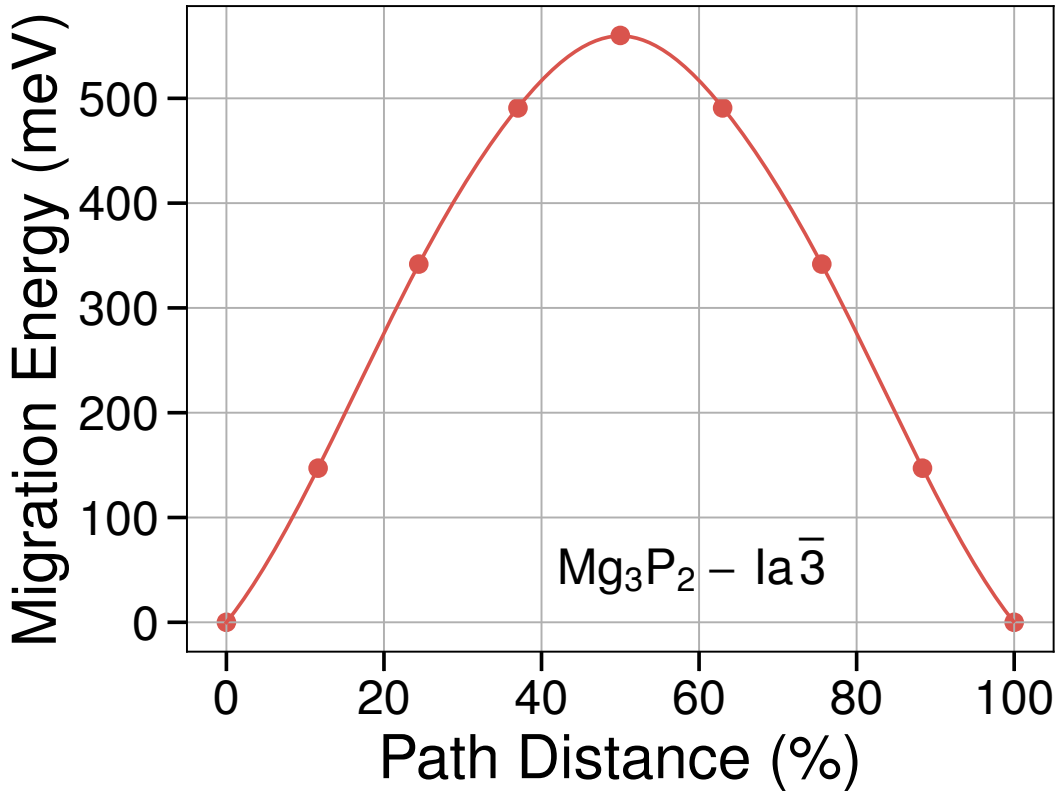
Migration Energy (meV)
500
400
300
200
100
0
$Mg_3P_2 - Ia\bar{3}$
0
20
40
60
80
100
Path Distance (%)

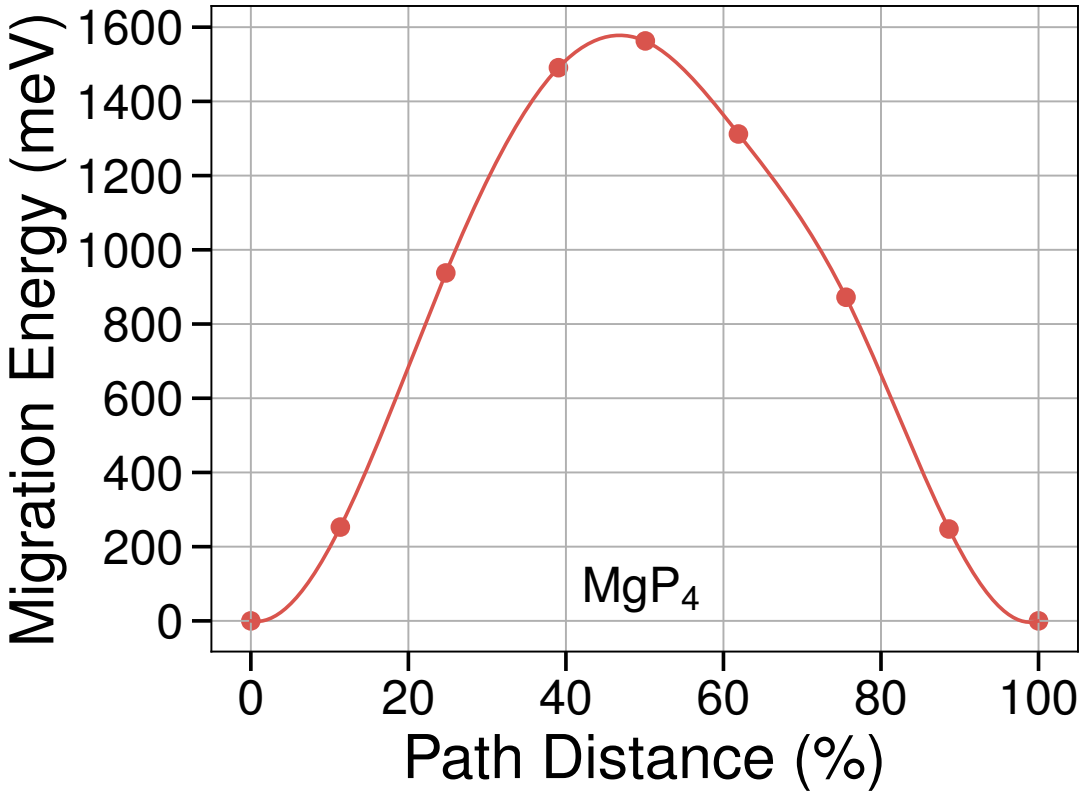
Migration Energy (meV)
1600
1400
1200
1000
800
600
400
200
0
MgP_4
0
20
40
60
80
100
Path Distance (%)

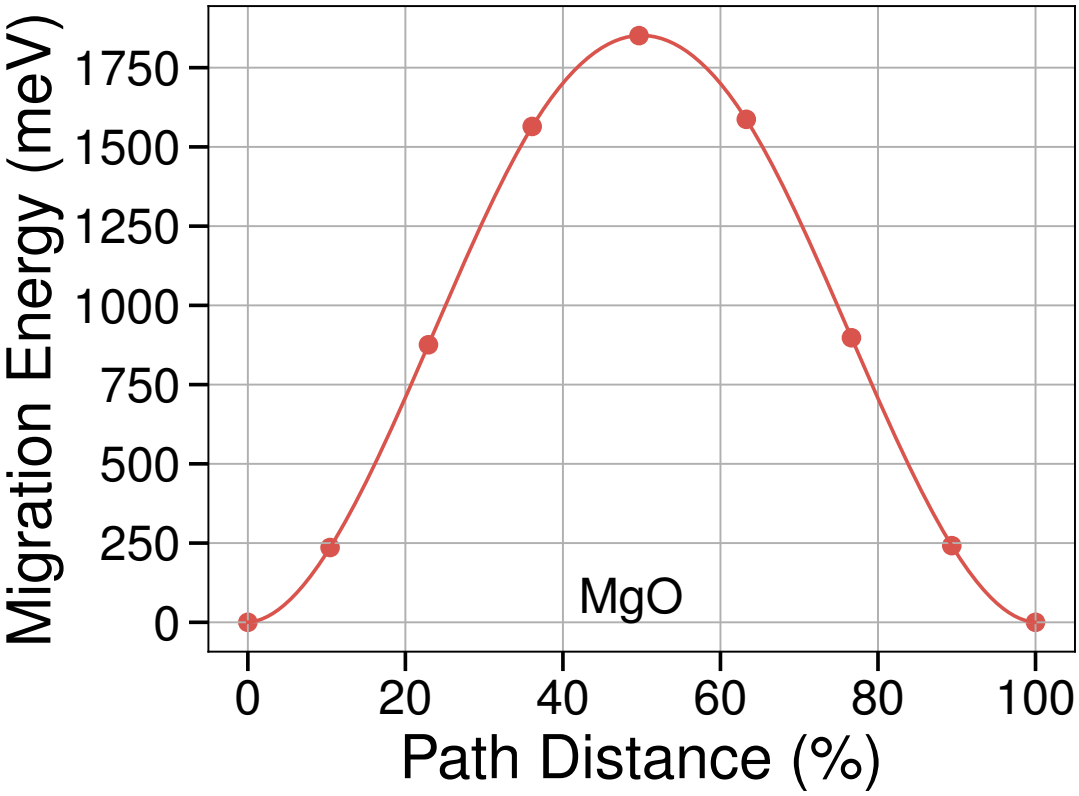
Migration Energy (meV)
1750
1500
1250
1000
750
500
250
0
MgO
0
20
40
60
80
100
Path Distance (%)

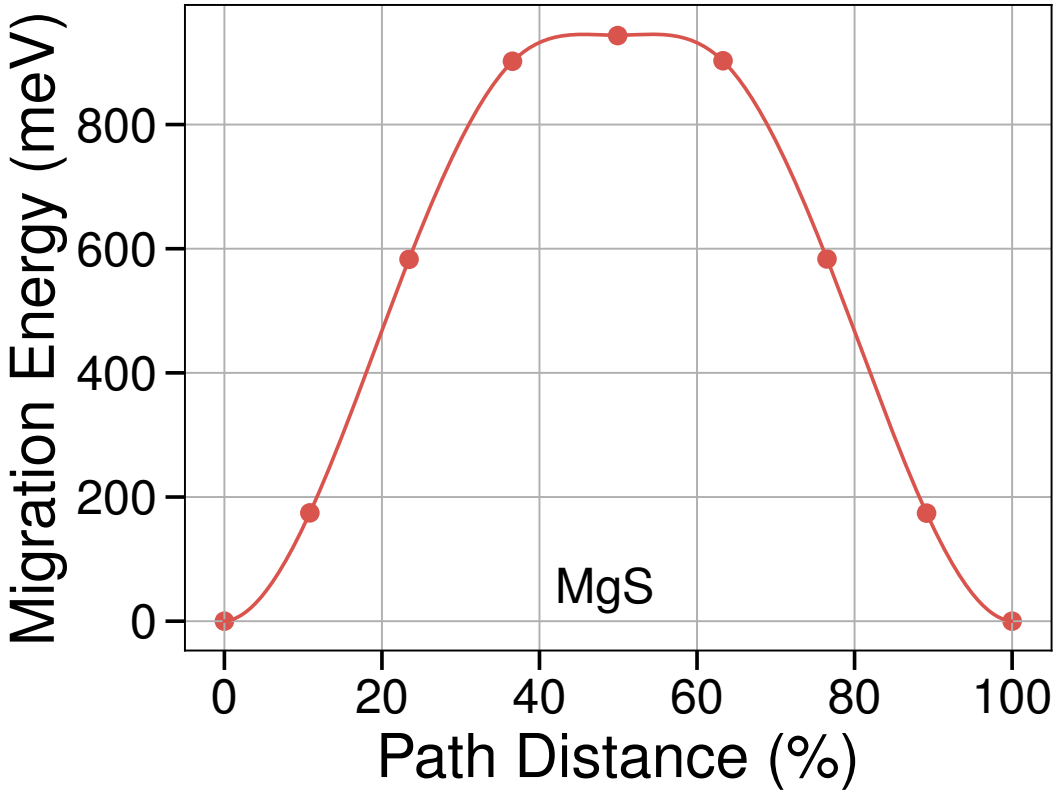
Migration Energy (meV)
800
600
400
200
0
MgS
0
20
40
60
80
100
Path Distance (%)

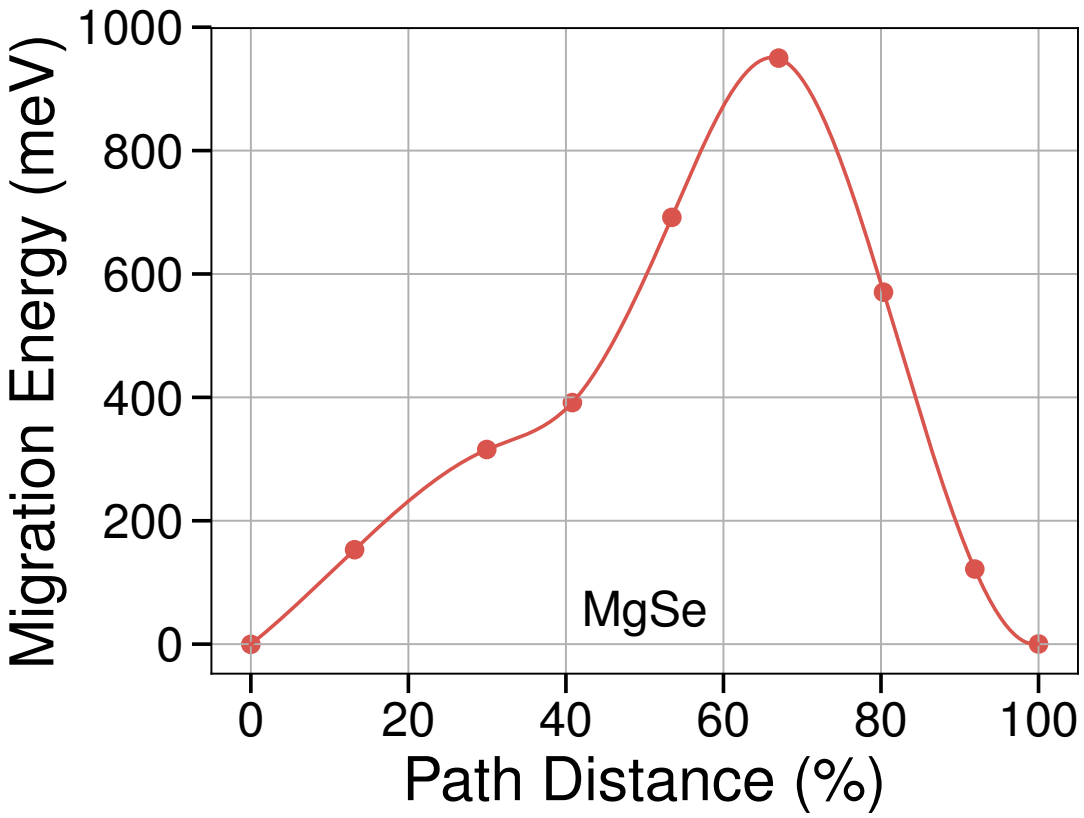
Migration Energy (meV)
1000
800
600
400
200
0
MgSe
0
20
40
60
80
100
Path Distance (%)

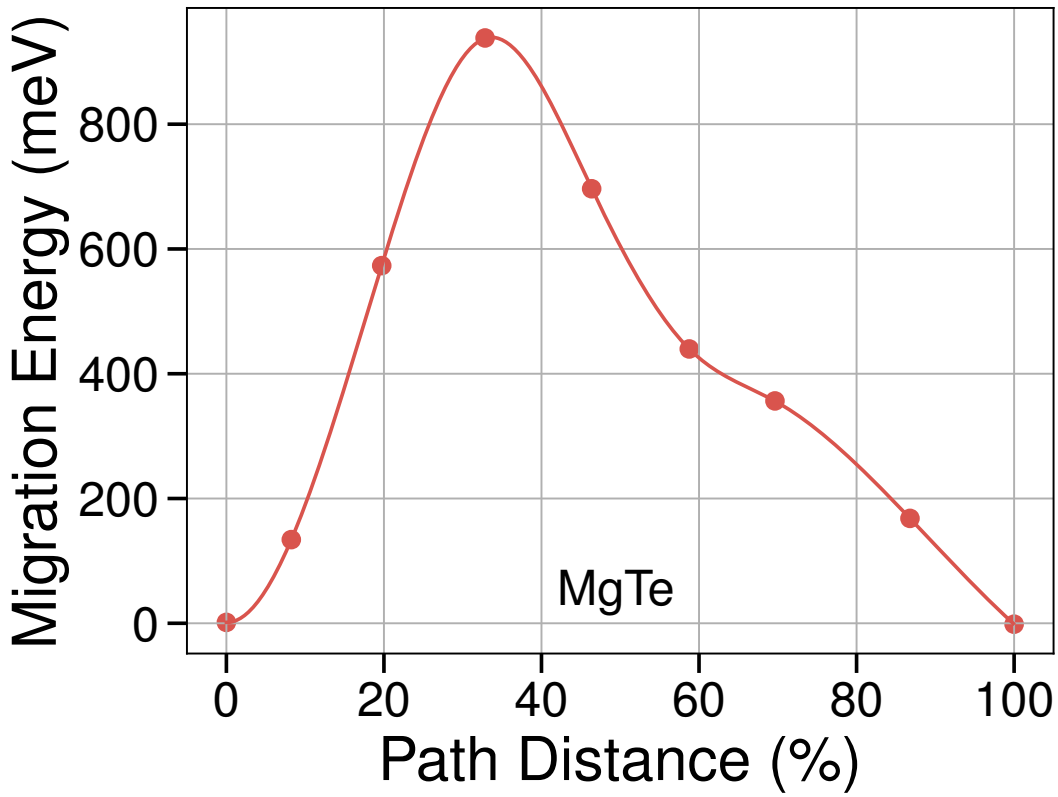
Migration Energy (meV)
800
600
400
200
0
MgTe
0
20
40
60
80
100
Path Distance (%)

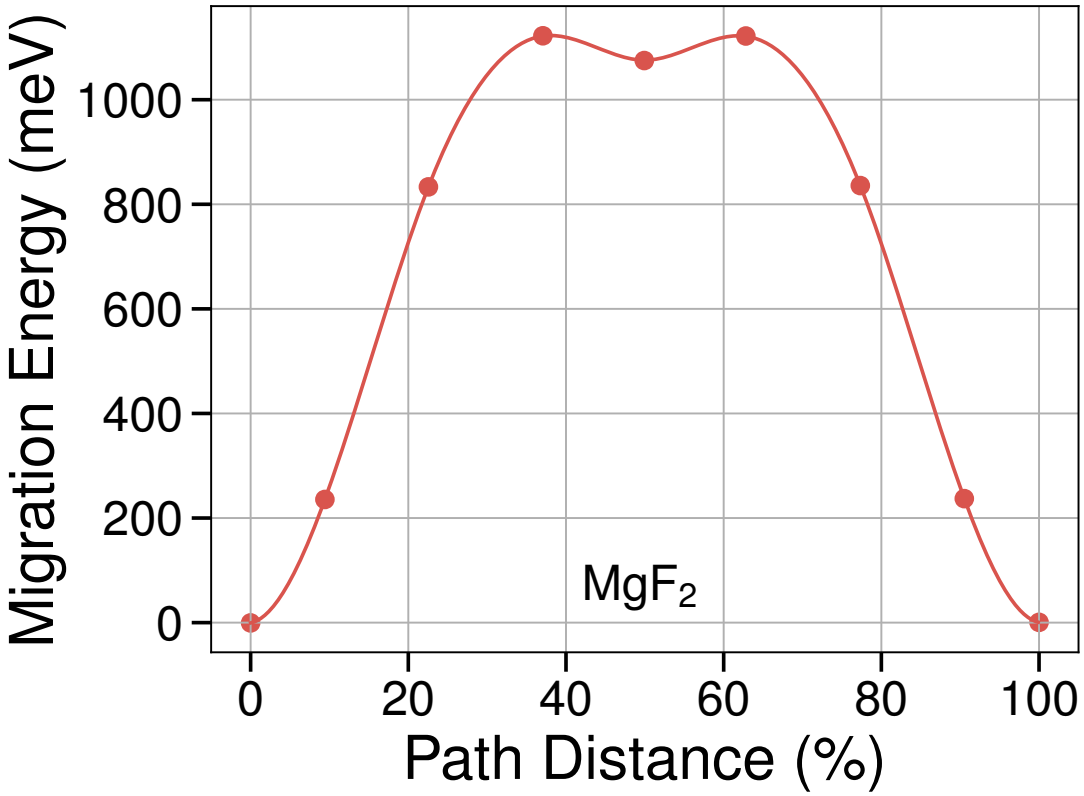
Migration Energy (meV)
1000
800
600
400
200
0
MgF2
0
20
40
60
80
100
Path Distance (%)

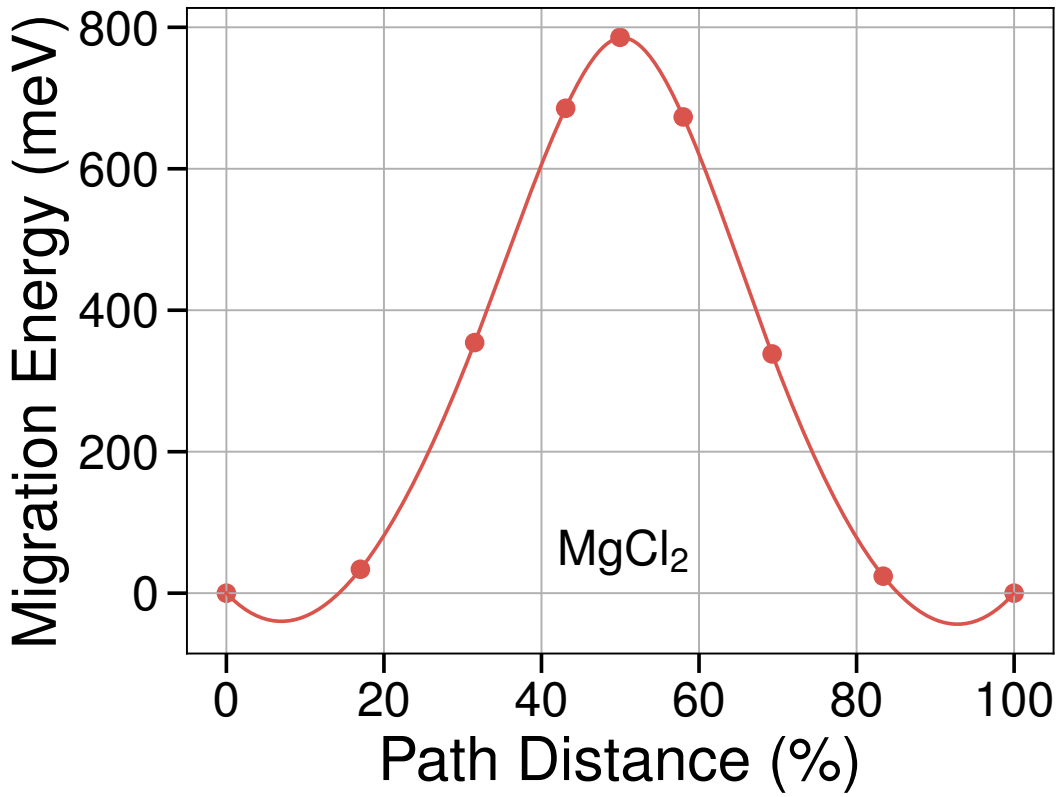
Migration Energy (meV)
800
600
400
200
0
MgCl2
0
20
40
60
80
100
Path Distance (%)

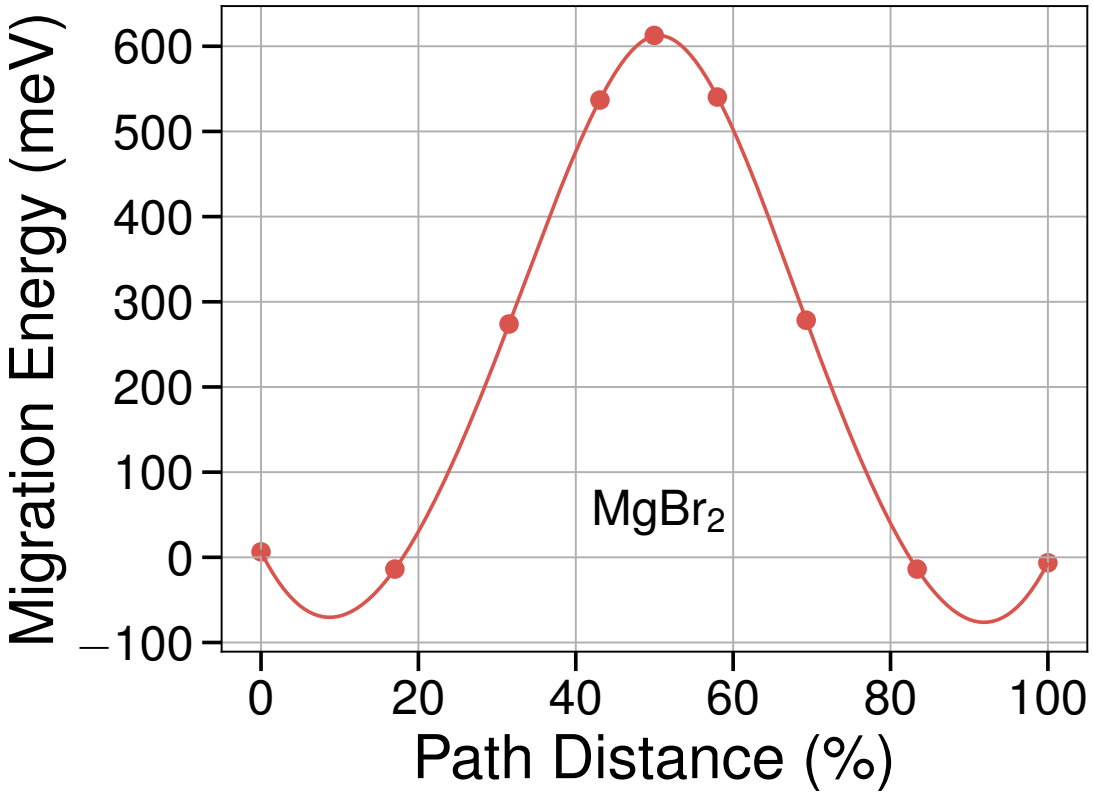
Migration Energy (meV)
600
500
400
300
200
100
0
−100
0
20
40
60
80
100
Path Distance (%)
MgBr2

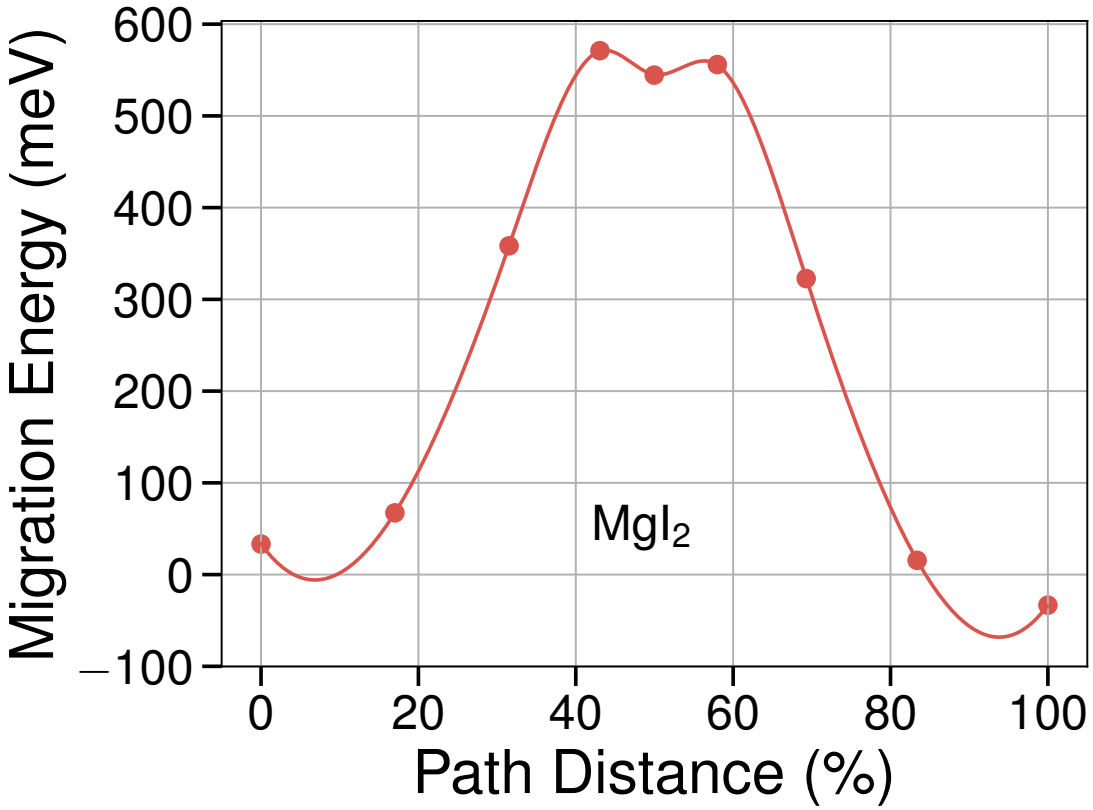
Migration Energy (meV)
600
500
400
300
200
100
0
−100
0
20
40
60
80
100
Path Distance (%)
MgI2

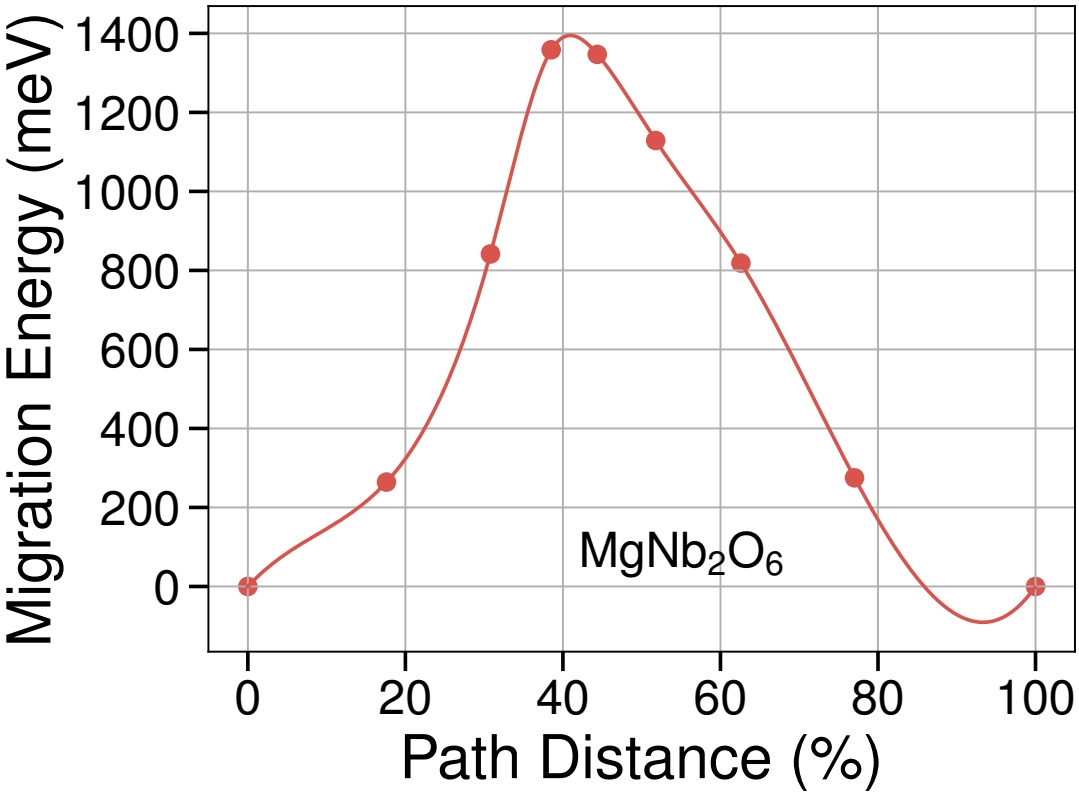
Migration Energy (meV)
1400
1200
1000
800
600
400
200
0
MgNb2O6
0
20
40
60
80
100
Path Distance (%)

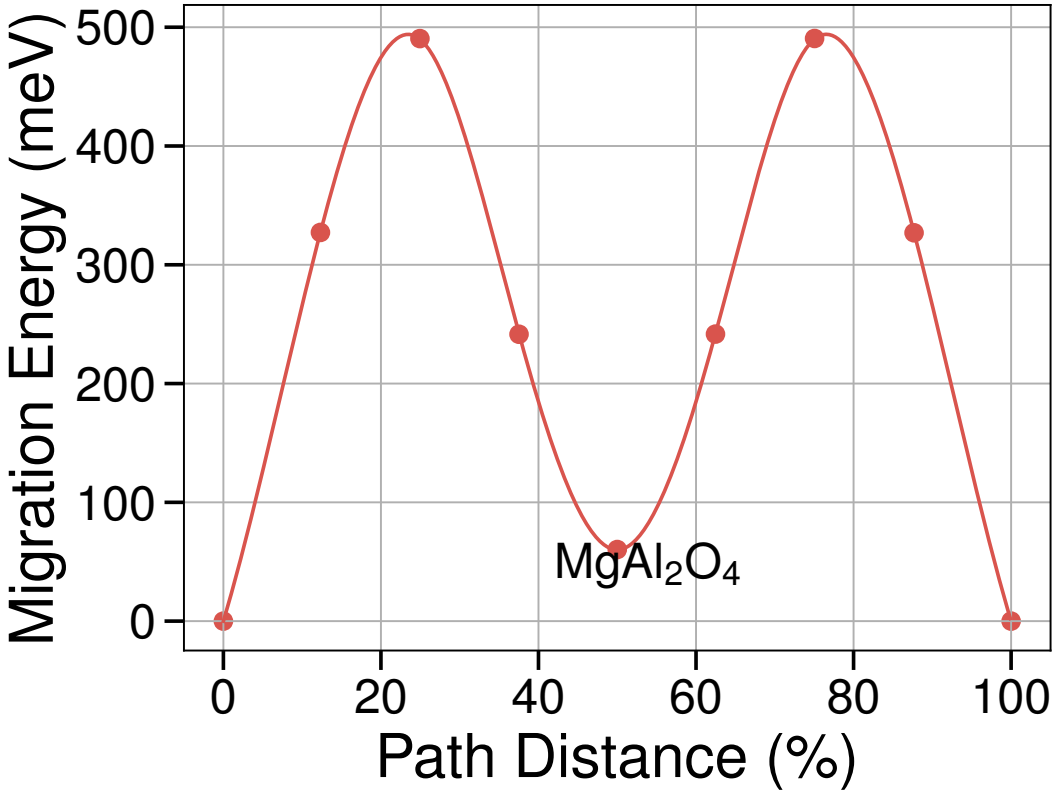
Migration Energy (meV)
500
400
300
200
100
0
MgAl2O4
0
20
40
60
80
100
Path Distance (%)

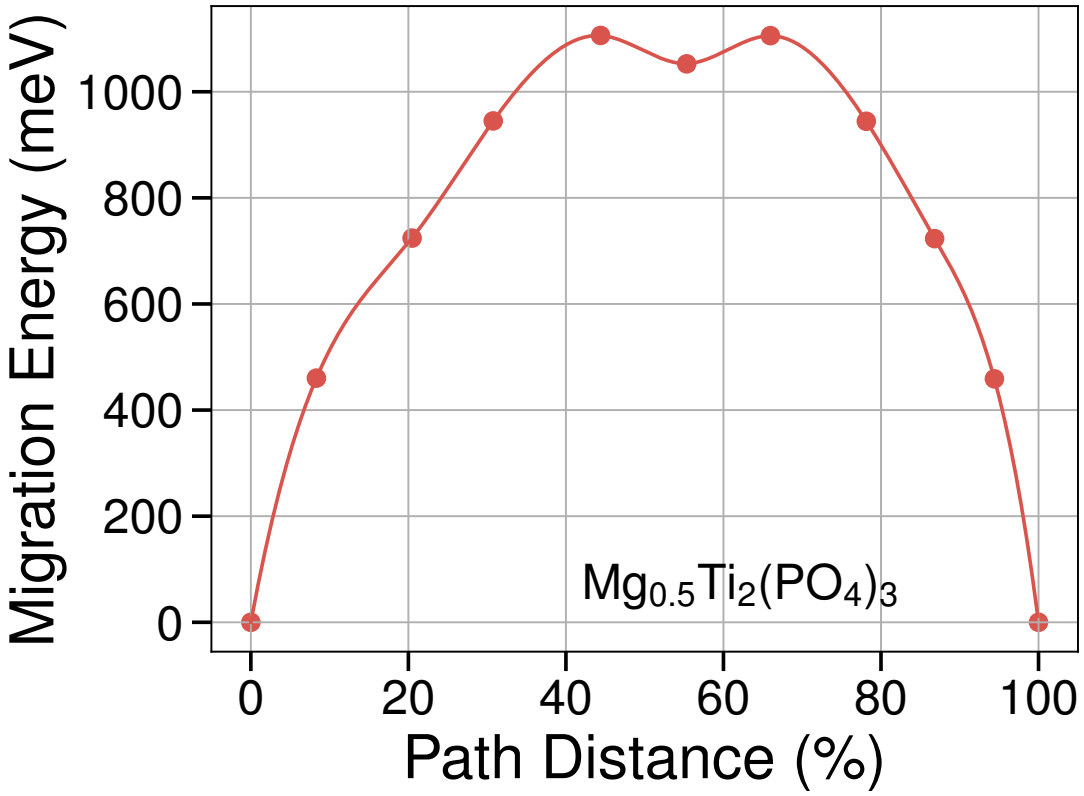
Migration Energy (meV)
1000
800
600
400
200
0
0
20
40
60
80
100
Path Distance (%)
$Mg_{0.5}Ti_2(PO_4)_3$

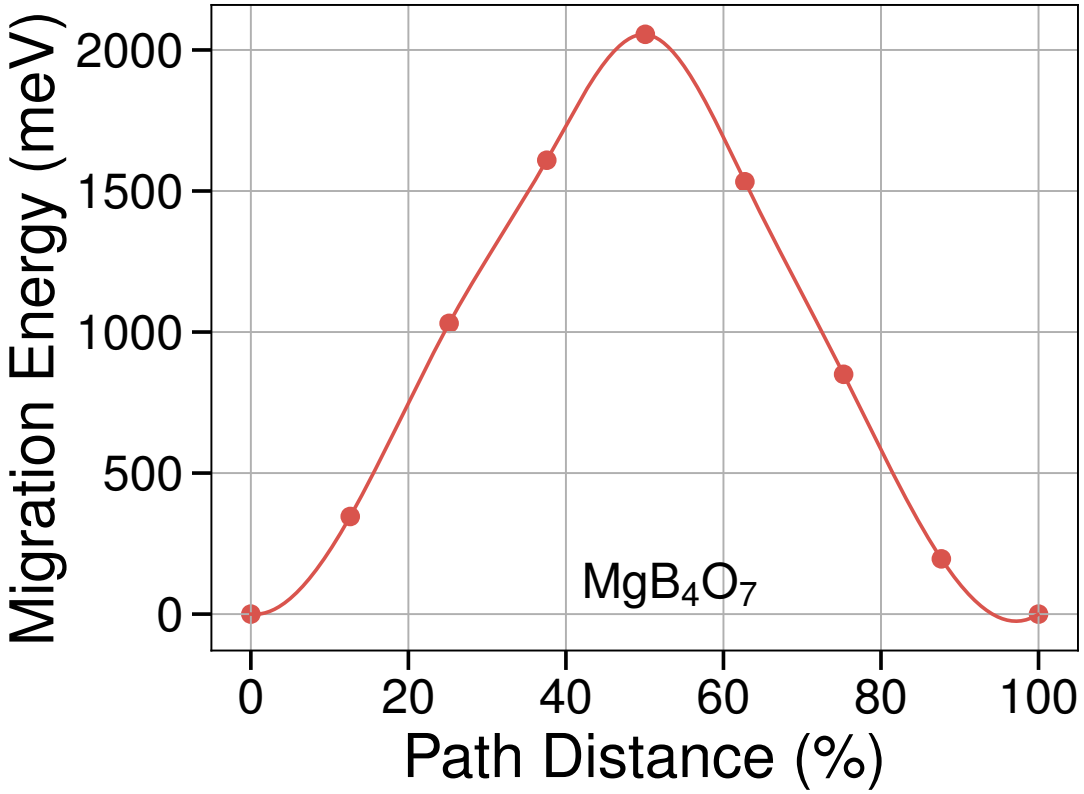
Migration Energy (meV)
2000
1500
1000
500
0
0
20
40
60
80
100
Path Distance (%)
MgB_4O_7

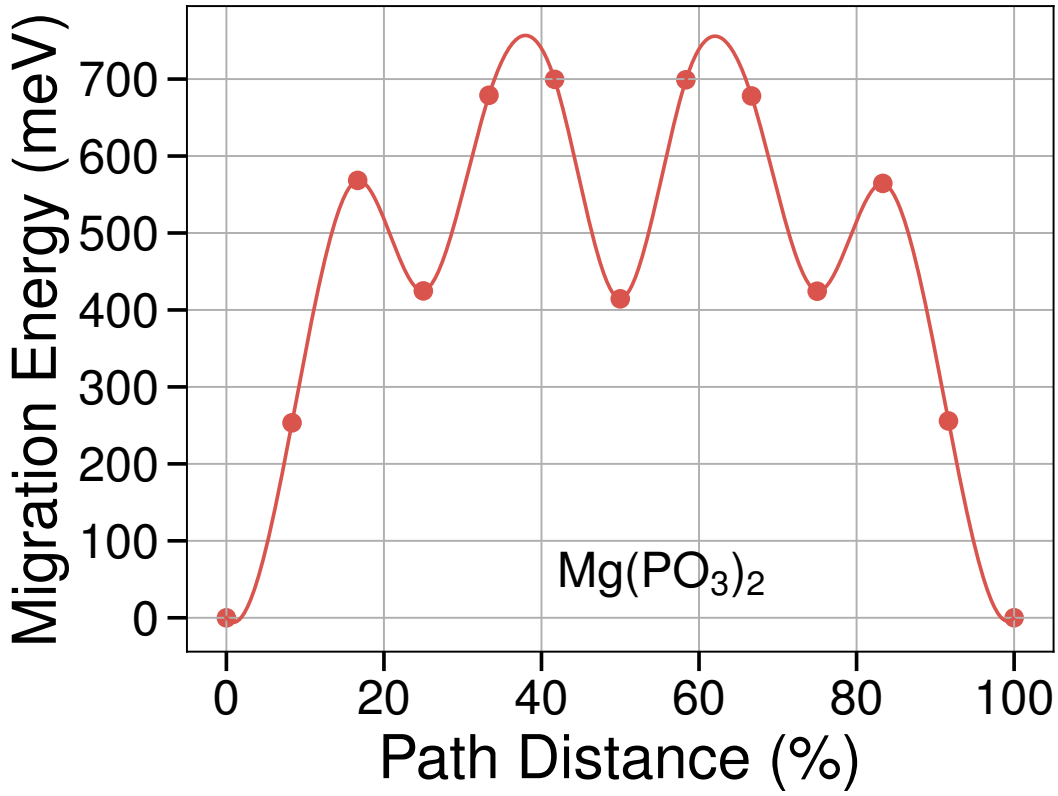
Migration Energy (meV)
700
600
500
400
300
200
100
0
0
20
40
60
80
100
Path Distance (%)
Mg(PO3)2

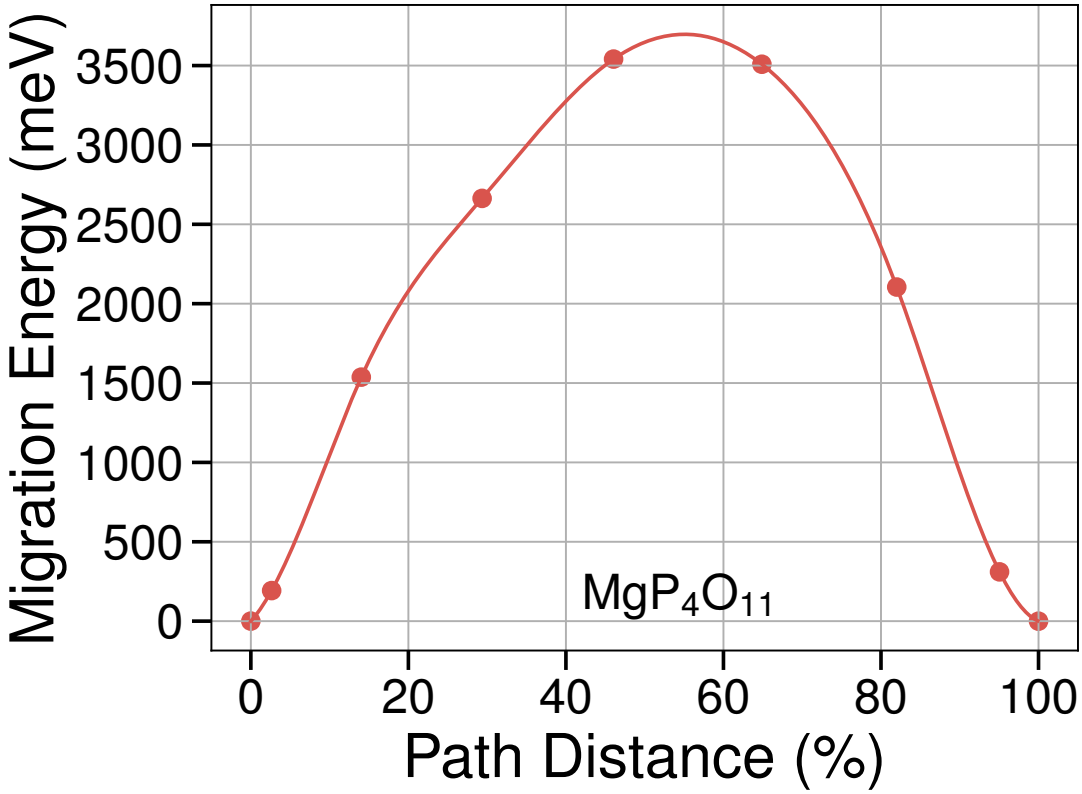
Migration Energy (meV)
3500
3000
2500
2000
1500
1000
500
0
0
20
40
60
80
100
Path Distance (%)
MgP4O11

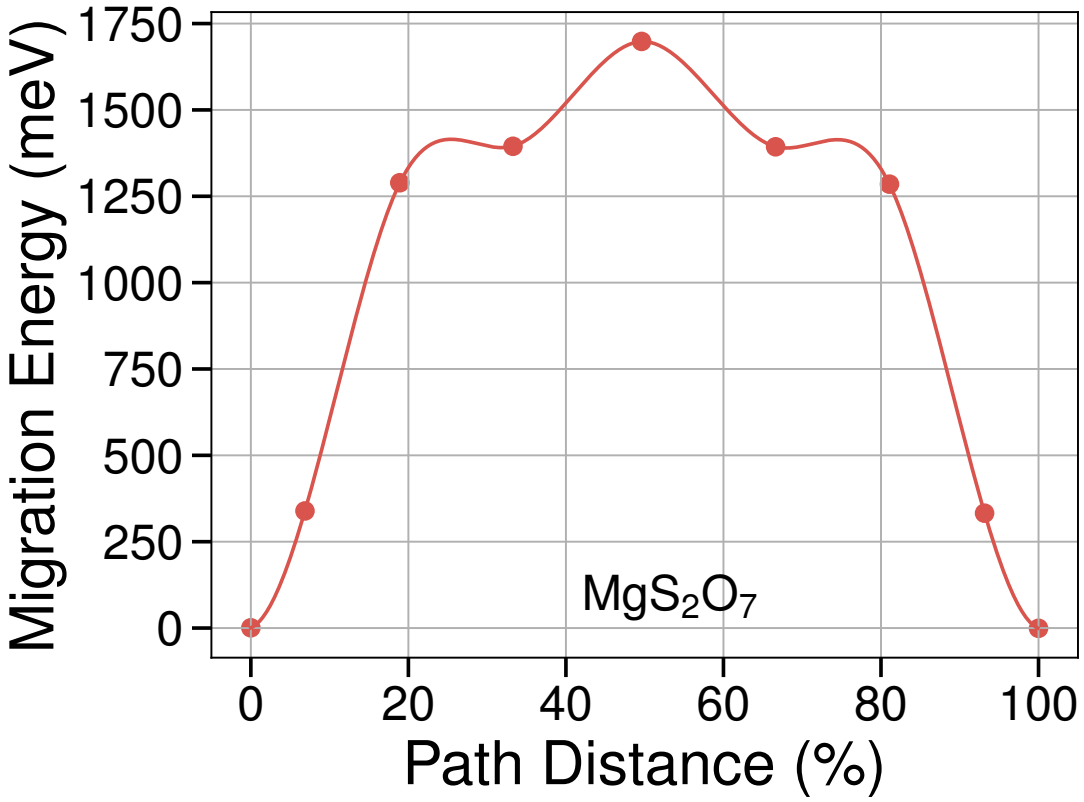
Migration Energy (meV)
1750
1500
1250
1000
750
500
250
0
0
20
40
60
80
100
Path Distance (%)
MgS_2O_7

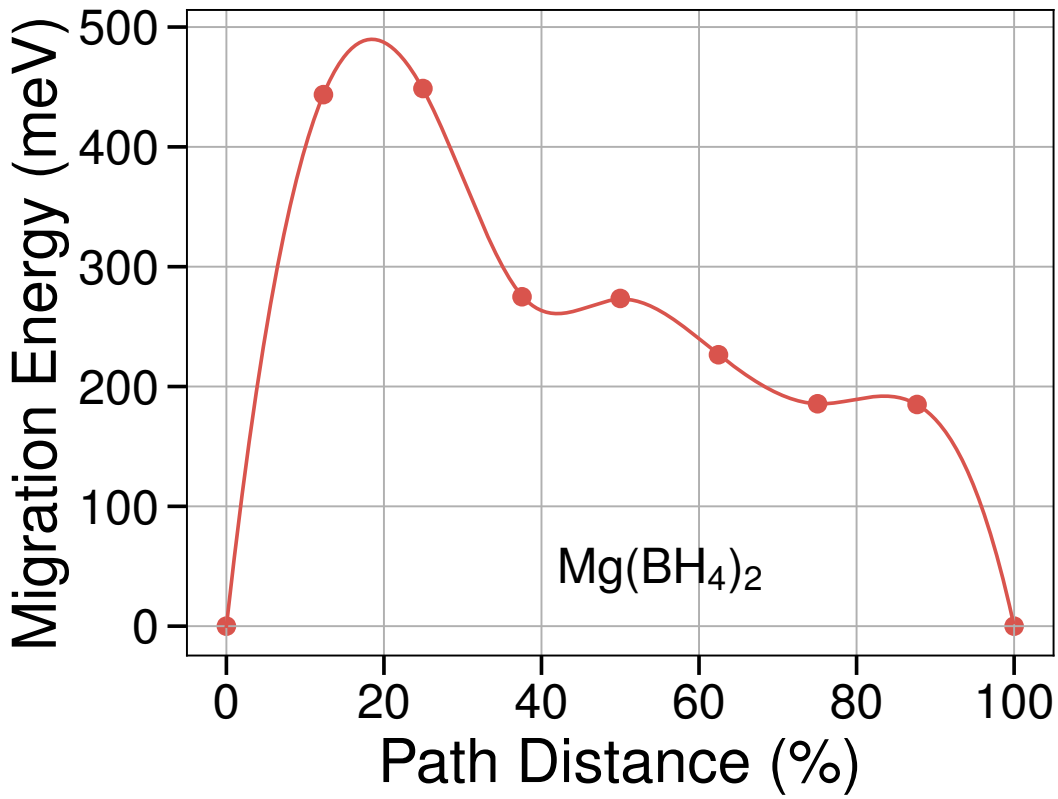
Migration Energy (meV)
500
400
300
200
100
0
0
20
40
60
80
100
Path Distance (%)
$Mg(BH_4)_2$

S2 Mg^{2+} Migration Energy Paths in Metastable Polymorphs

We also calculated the Mg migration barriers in a few metastable structures at the compositions of Mg_3P_2 (space group: $Pn\bar{3}m$; Materials Project ID: mp-8085), Mg_2Si ($P6_3/mmc$; mp-1018796), $MgSe_2$ ($Pa\bar{3}$; mp-1103590), and $MgTe_2$ ($Pa\bar{3}$; mp-2604), as reported below.

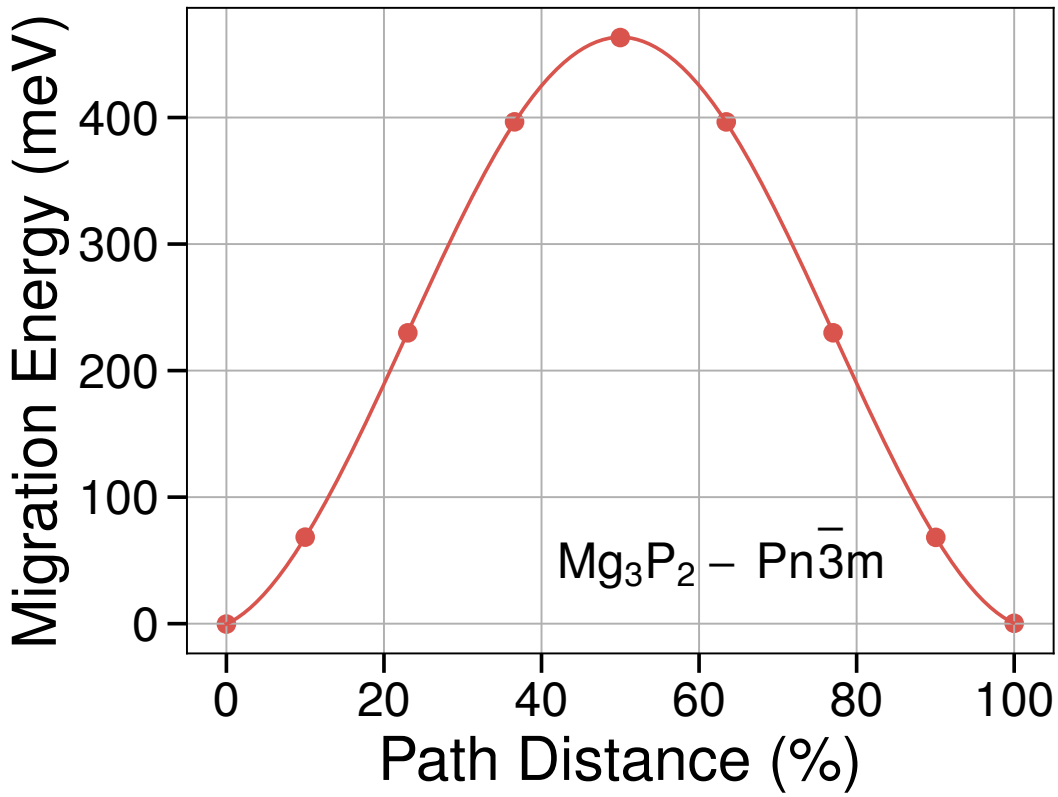

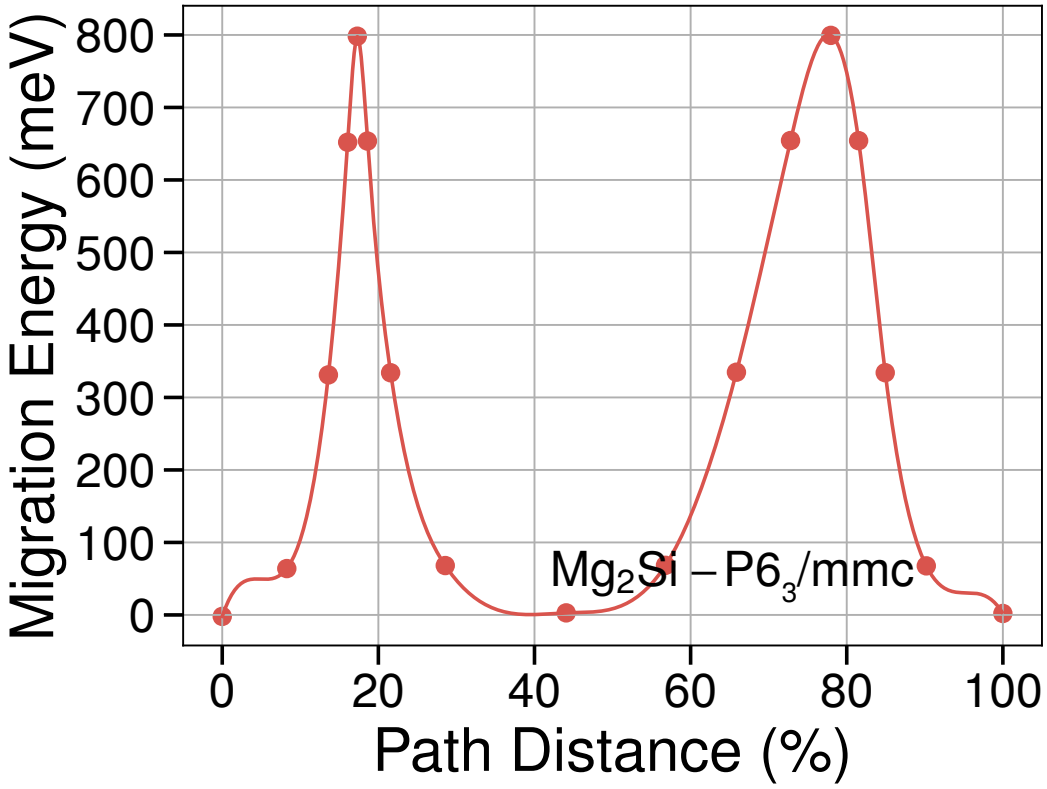
Migration Energy (meV)
800
700
600
500
400
300
200
100
0
0
20
40
60
80
100
Path Distance (%)
Mg2Si – P63/mmc

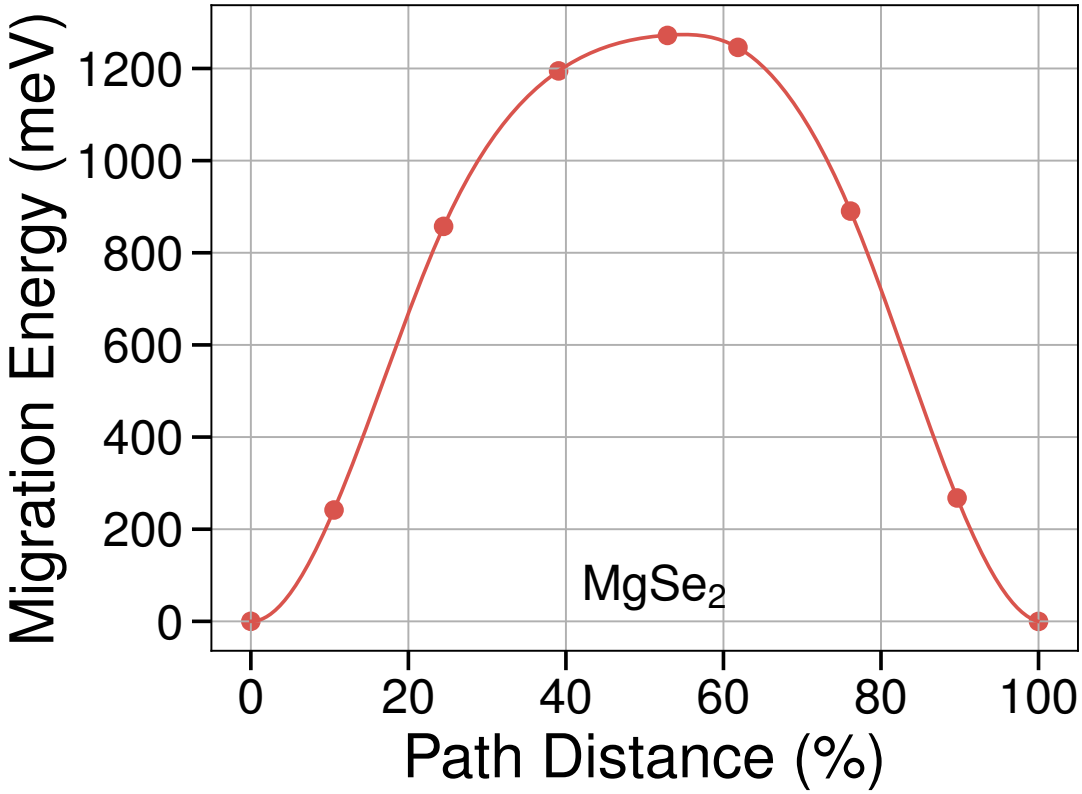
Migration Energy (meV)
1200
1000
800
600
400
200
0
0
20
40
60
80
100
Path Distance (%)
MgSe2

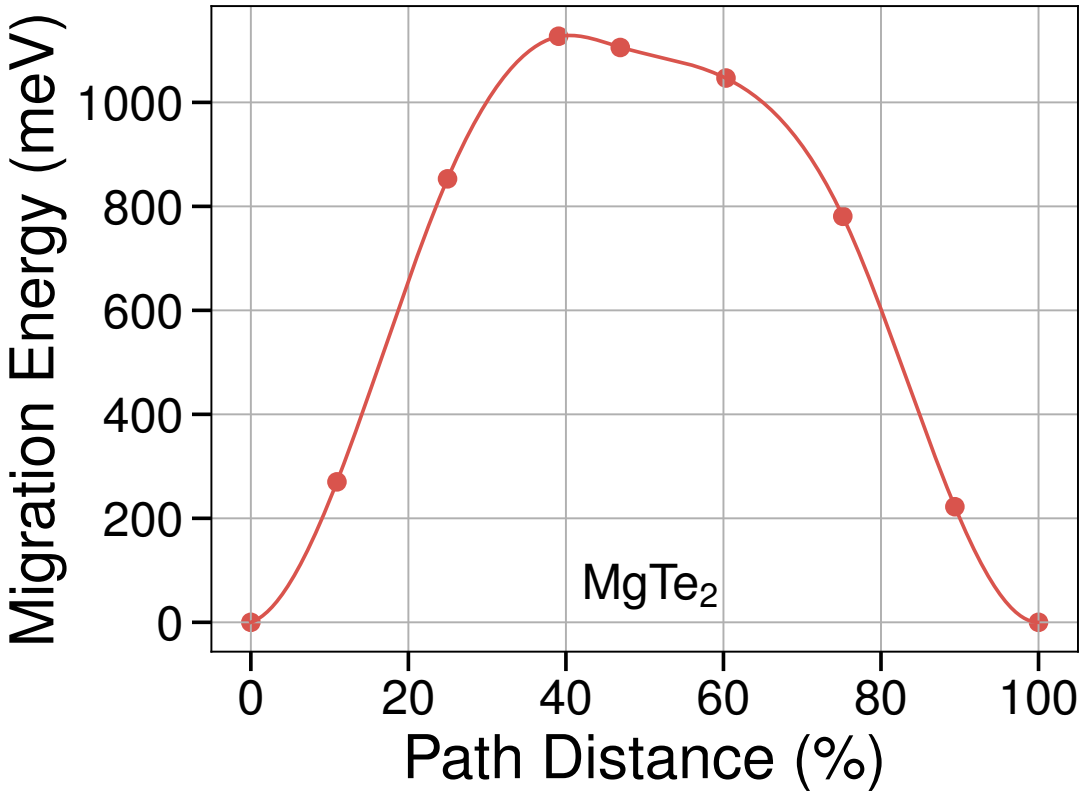
Migration Energy (meV)
1000
800
600
400
200
0
MgTe2
0
20
40
60
80
100
Path Distance (%)

S3 Convergence of Migration Barriers vs. Finite-size effects

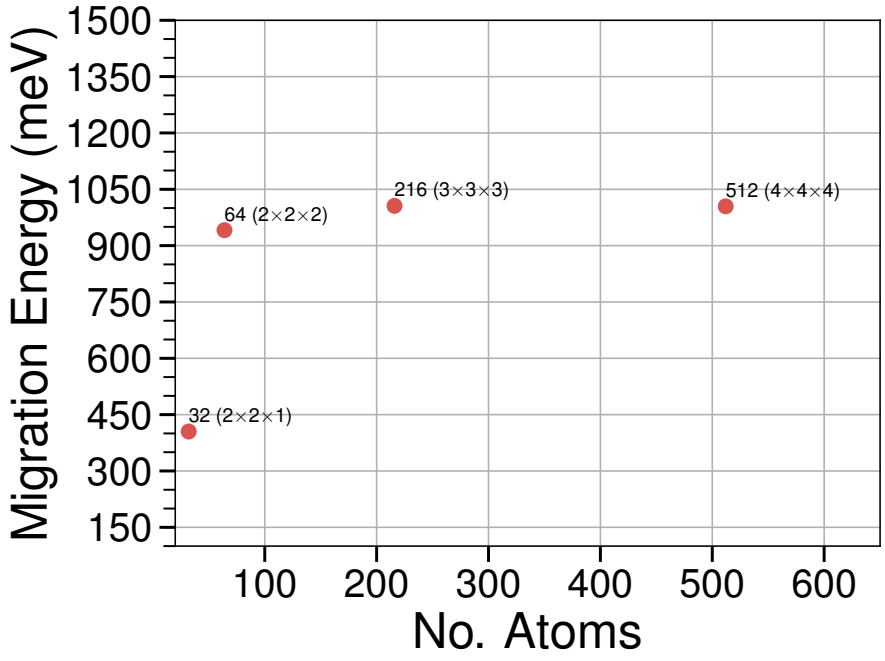

Figure S1 Migration barriers (in meV) of Mg in MgS as the size of the simulation cell is varied. The specific simulation cell used (in brackets) and the number of atoms within the pristine cell are indicated by the text near each data point.

Figure S1 shows the calculated Mg^{2+} migration barriers in MgS including the background charge at varying supercell size. Starting from a conventional cell with dimensions of 5.23×5.23×5.23 $Å^3$, we perform nudged elastic band (NEB) calculations using supercells of size 2×2×1 (32 atoms without Mg vacancy) of the conventional cell up to 4×4×4 (512 atoms). While the migration barrier within a 2×2×1 supercell (~400 meV) exhibits significant deviation (~600 meV) from the 4×4×4 supercell (~1000 meV), the migration barrier using the 2×2×2 supercell (~950 meV) is only slightly lower than the 4×4×4 (by ~50 meV). Note that ±50 meV is the typical error bar in the estimation of our migration barriers, which corresponds to ±1 order of magnitude in diffusivity, in agreement with the typical uncertainty in experiments (e.g., migration barrier estimates via galvanostatic intermittent titration measurements). Thus, using a supercell size of 2×2×2 gives a converged Mg^{2+} migration barrier.

S4 Electrostatic corrections to evaluate the formation energy of charge-compensated Mg Vacancies

The following plots depict the electrostatic correction schemes used for computing the charge-compensated Mg-vacancy ($V''_{\mathrm{Mg}}, q = -2$) formation energies, listed in Table 2 of the main text for $MgAl_2O_4$ (**Figure S2**), $MgBr_2$ (**Figure S3**), and $MgSiN_2$ (**Figure S4**). We used the methodology proposed by Freysoldt *et al.*[1] for the isotropic $MgAl_2O_4$ (cubic), whereas both $MgBr_2$ (hexagonal) and $MgSiN_2$ (orthorhombic) being anisotropic materials required the scheme proposed by Kumagai and Oba.[2] Both correction schemes involve correcting long-range interactions by calculating the electrostatic potential using a classical model (e.g., using point-charges or Gaussians), while the short-range interactions are corrected by a constant shift such that the electrostatic potential "far away" from the defect becomes zero. Thus, both correction schemes are considered converged if the difference in the electrostatic potential between the defective structure, the pristine bulk, and the classical model decays to a constant non-zero value far away from the defect. Note that the long-range potential needs to be scaled by the dielectric constant (ϵ) of the pure bulk structure, which we calculated using density functional perturbation theory (employing the Perdew-Burke-Ernzerhof exchange-correlation functional) and have listed in **Table S1**. Captions for the figures below contain descriptions of the various data that are being plotted, supercell sizes used in calculations, and the actual correction values used to evaluate vacancy formation energies.

Material	Contribution	ϵ_{xx}	ϵ_{yy}	ϵ_{zz}
$MgAl_2O_4$	Electronic	3.08		
	Ionic	5.05		
$MgBr_2$	Electronic	3.22		2.60
	Ionic	3.19		0.42
$MgSiN_2$	Electronic	4.40	4.35	4.27
	Ionic	5.31	4.19	3.62

Table S1: Dielectric constants for the bulk materials. The sum of electronic and ionic contributions to the dielectric constant is used for estimating the electrostatic correction. The off-diagonal components (ϵ_{ij}) are ~0 for all materials listed.

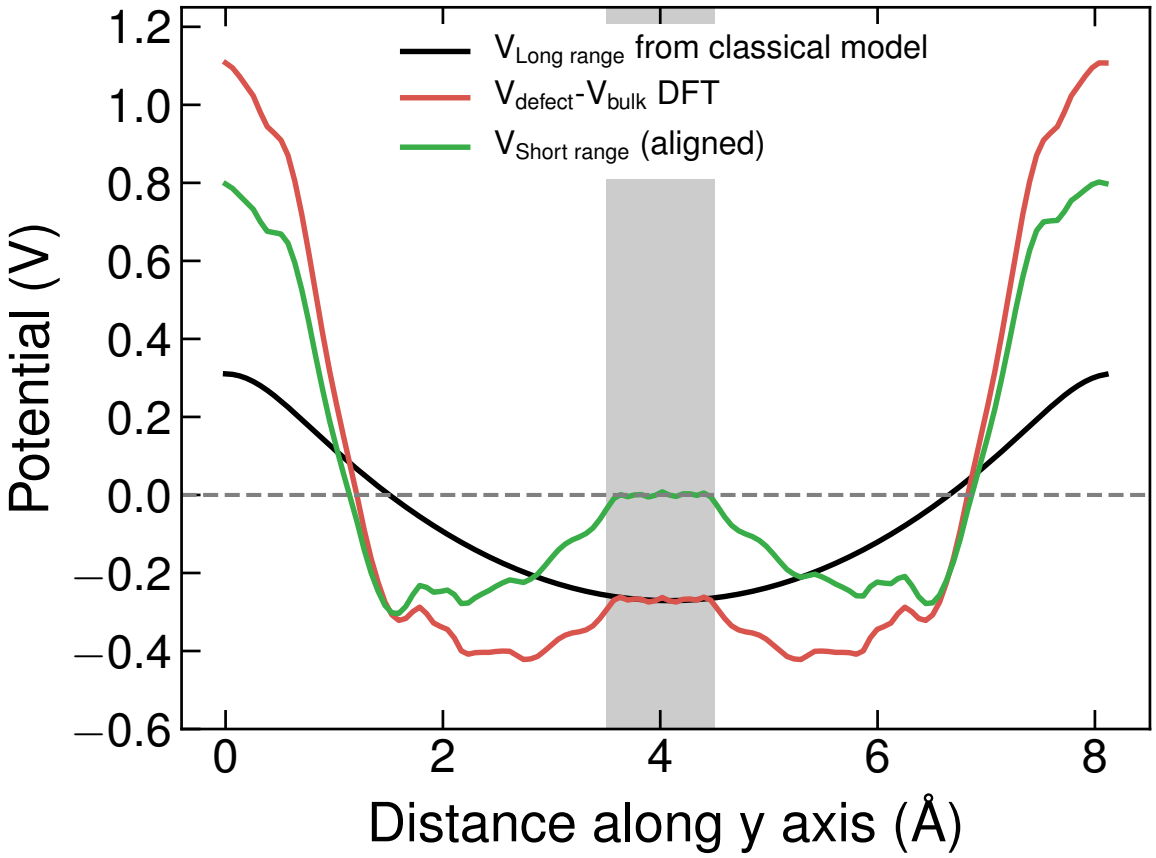

Figure S2 Correction scheme of Freysoldt *et al.* to account for spurious electrostatic interactions in $MgAl_2O_4$ with a charge-compensated Mg-vacancy. $V_{Long\ range}$ (black line) is the planar-averaged electrostatic potential evaluated by a Gaussian model of charges ($q = -2$), including the defect, i.e., the defect and its periodic images. Note that $V_{Long\ range}$ plotted here already includes the constant shift (C~0.045 V) for the short range term. $V_{defect} - V_{bulk}$ (red line) is the difference in the planar-averaged electrostatic potential of the defective and pristine bulk structures, as computed by DFT. Thus, $V_{defect} - V_{bulk}$ includes the spurious electrostatic interactions between the defect site, its periodic images, and the compensating background charge. $V_{Short\ range}$ (green line) indicates the difference between $V_{defect} - V_{bulk}$ and $V_{Long\ range}$, and the constant shift required to determine the short range correction is nominally obtained by sampling the uncorrected short range potential far away from the defect (indicated by the grey shaded area). Since the corrected short range potential (green line) is ~0 V within the sampling region, we consider our charged defect calculation to be well-converged. Including the long range (~1.23 eV) and short range (~0.09 eV) contributions, the final correction (E_{corr}) for V''_{Mg} in $MgAl_2O_4$ is ~1.32 eV. We used the conventional $MgAl_2O_4$ cell to evaluate the total energies and electrostatic potentials of the defective and pristine configurations.

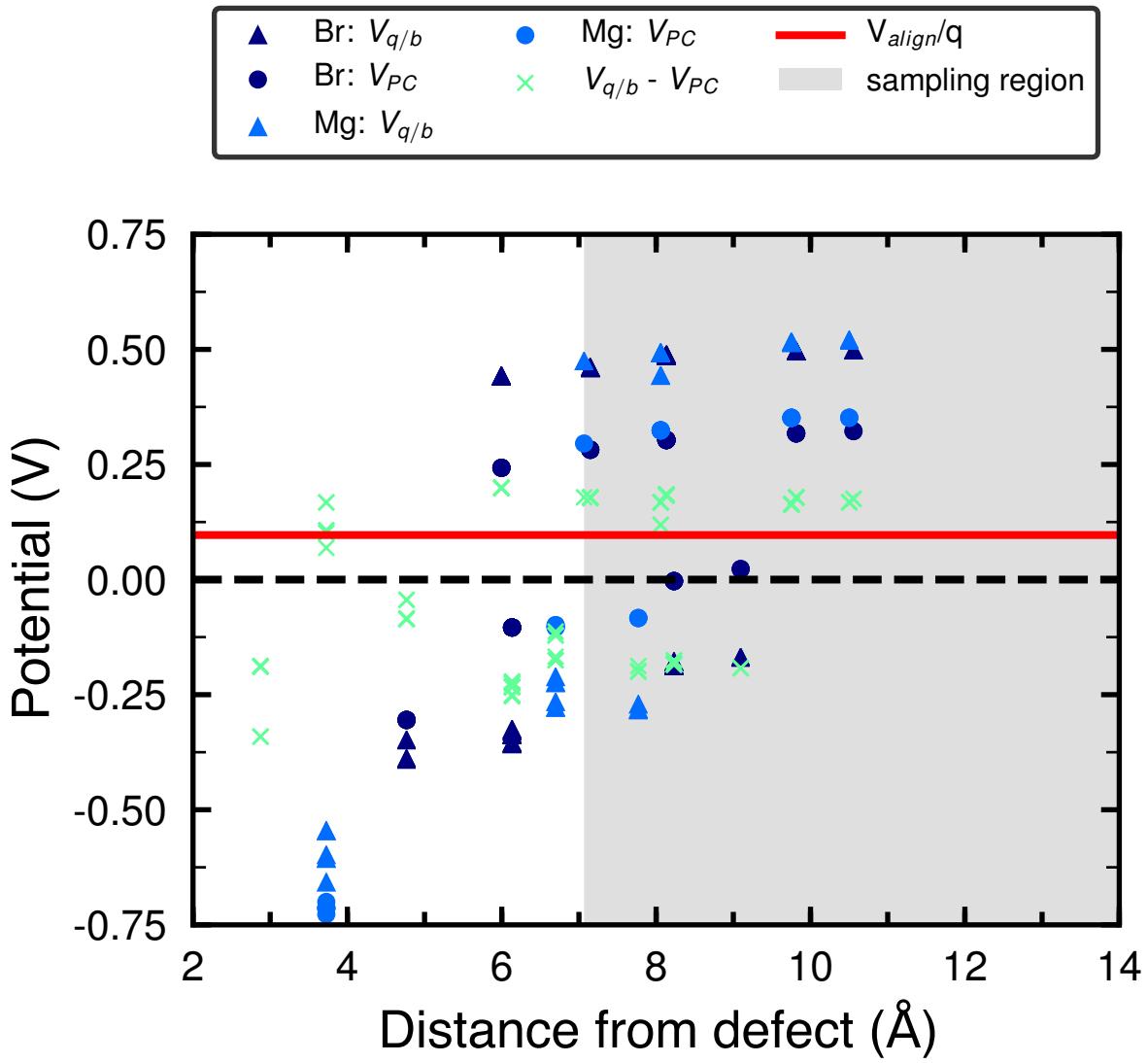

Figure S3 Correction scheme of Kumagai and Oba to account for spurious electrostatic interactions in $MgBr_2$ with a charge-compensated Mg-vacancy. V_{PC} (circles) is the long-range electrostatic potential evaluated using a point-charge (PC) model (including V''_{Mg}) of the periodically repeating defect. $V_{q/b}$ (triangles) is the difference in the electrostatic potential computed by DFT between the defective (q) and pristine (b) structures. Both V_{PC} and $V_{q/b}$ are calculated at atomic positions corresponding to Mg (light blue) and Br (dark blue) atoms within $MgBr_2$. The green crosses ($V_{q/b}$ – V_{PC}) indicate the difference between the DFT-computed electrostatic potential and the potential derived from the PC model. The values of $V_{q/b}$ – V_{PC} are sampled (grey area) at atomic sites within the Wigner-Seitz cell of $MgBr_2$, and averaged to obtain the alignment term (V_{align}/q, solid red line), which represents the required short-range correction. Including the long range (~1.10 eV) and short range (~0.19 eV) contributions yields an electrostatic correction (E_{corr}) value of ~1.29 eV for V''_{Mg} in $MgBr_2$. We used a 4×4×2 supercell of the conventional $MgBr_2$ structure to evaluate the total energies and electrostatic potentials of the defective and pristine configurations.

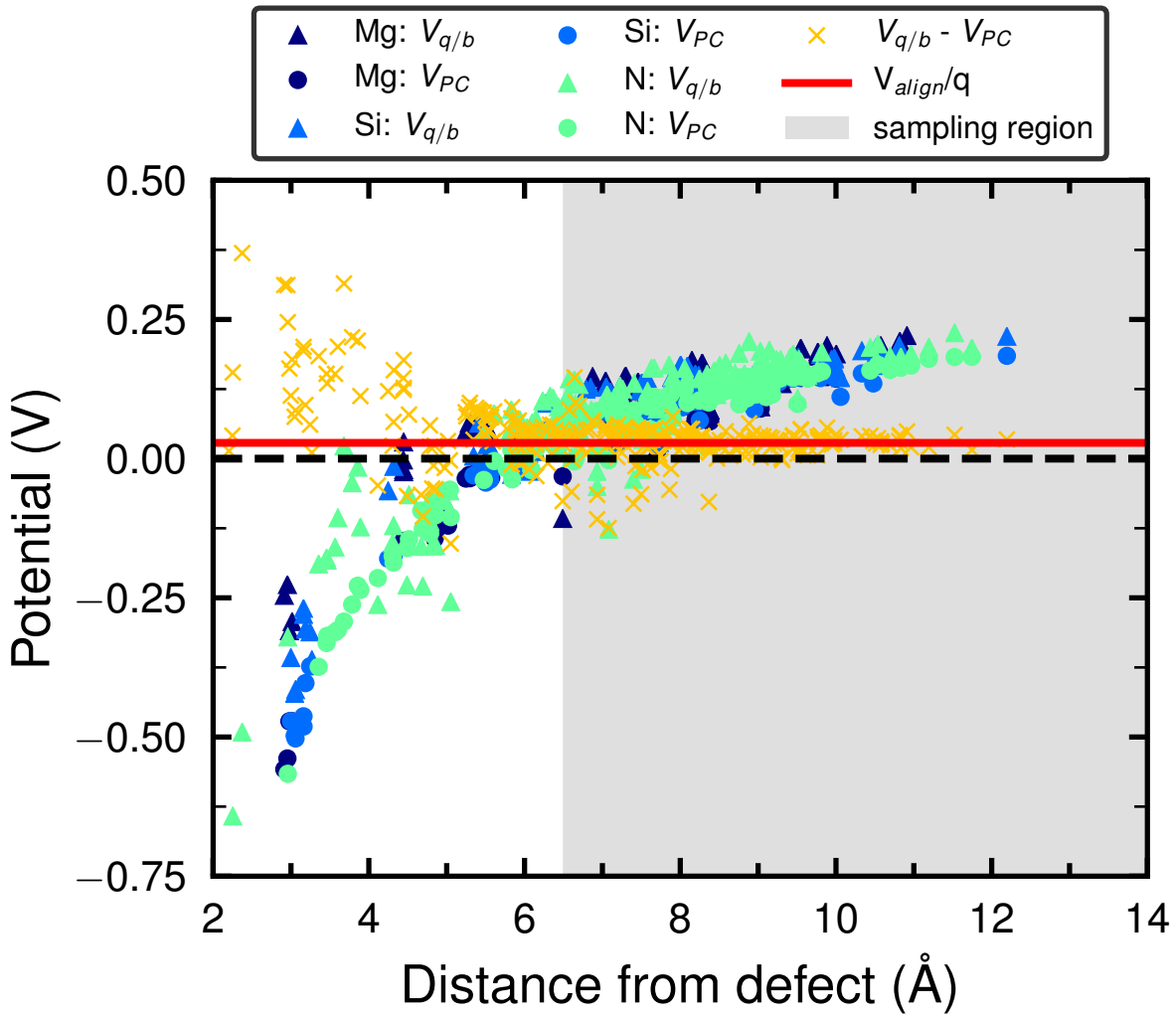

Figure S4 Correction scheme of Kumagai and Oba to account for spurious electrostatic interactions in $MgSiN_2$ with a charge-compensated Mg-vacancy. V_{PC} (circles) is the long-range electrostatic potential evaluated using a point-charge model (including V''_{Mg}) and $V_{q/b}$ (triangles) is the difference in the electrostatic potential (from DFT) between the defective (q) and pristine (b) structures. V_{PC} and $V_{q/b}$ are calculated at atomic positions corresponding to Mg (dark blue), Si (light blue) and N (green) atoms. Yellow crosses ($V_{q/b}$ – V_{PC}) indicate the difference between the DFT-computed electrostatic potential and the point-charge model potential, which are sampled (grey area) at atomic sites within the Wigner-Seitz cell of $MgSiN_2$, and averaged to obtain the short-range alignment term (V_{align}/q, solid red line). Including the long range (~0.64 eV) and short range (~0.06 eV) contributions yields an electrostatic correction (E_{corr}) value of ~0.70 eV for V''_{Mg} in $MgSiN_2$. We used a 3×3×2 supercell of the conventional $MgSiN_2$ structure to evaluate the total energies and electrostatic potentials of the defective and pristine configurations.

References

(1) Freysoldt, C.; Neugebauer, J.; Van De Walle, C. G. Fully Ab Initio Finite-Size Corrections for Charged-Defect Supercell Calculations. *Phys. Rev. Lett.* **2009**, *102* (1), 1–4. https://doi.org/10.1103/PhysRevLett.102.016402.

(2) Kumagai, Y.; Oba, F. Electrostatics-Based Finite-Size Corrections for First-Principles Point Defect Calculations. *Phys. Rev. B* **2014**, *89* (19), 195205. https://doi.org/10.1103/PhysRevB.89.195205.